Journal of Electroanalytical Chemistry 947 (2023) 117791

Contents lists available at ScienceDirect

Journal of Electroanalytical Chemistry

journal homepage: www.elsevier.com/locate/jelechem

Comparative electrochemical behavior of Prussian blue analogues as a host electrode for rare earth element recovery

Rosalinda Sciacca [a], Mario Berrettoni [b], Paolo Conti [b], Marco Giorgetti [c,*]

[a] University of Bologna, Department of Industrial Chemistry "Toso Montanari", UOS, Campus di Rimini, Università di Bologna, Italy
[b] School of Science and Technology, Chemistry Division, "Chemistry Interdisciplinary Project" Building, University of Camerino, Camerino, Italy
[c] University of Bologna, Department of Industrial Chemistry "Toso Montanari", Viale del Risorgimento 4, 40136 Bologna, Italy

ARTICLE INFO

Keywords:
Copper Hexacyanoferrate thin film
Nickel Hexacyanoferrate thin film
Rare earth elements
Ion exchange kinetic mechanism

ABSTRACT

In this paper, electrodeposited films belonging to the Prussian Blue Analogues (PBAs) family, namely, nickel-hexacyanoferrate (NiHCF) and copper-hexacyanoferrate (CuHCF), were employed as a host material for rare earth elements (REE), and the reported insertion/release study reveals a recovery capability for such valuable metals. The ion insertion/release was accomplished by adopting an electrochemically-driven process. A reversible intercalation was observed while considering both heavy and ligth rare earth elements. The amount of REEs inserted/released over the process and its kinetic evolution during the process were also studied by a chemometric approach. For CuHCF, it was seen that the intercalation of heavy rare earth elements occurs easily respect to the light ones, suggesting a possible selectivity among these ions.

1. Introduction

Metal-hexacyanoferrates or Prussian Blue Analogues (MHCFs or PBAs) are an important class of mixed-valence compounds of great interest because of their electrocatalytic, ion-exchanging, ion-sensing, and photomagnetic properties [1], as well as for battery material, recently [2,3]. The conventional method to prepare PBAs includes simple chemical [4] or electrochemical deposition [5]. Among the metal hexacyanoferrates, nickel hexacyanoferrate (NiHCF) and copper hexacyanoferrate (CuHCF) are the most commonly used for alkali cations insertion capabilities. They are particularly used for trivalent cations intercalation [6–10] and as excellent candidates for cation selective extractions [11–15]. Indeed, the distinctive architecture of PBAs, characterized by a cubic framework with large zeolite-like interstitial sites, make these compounds able to easily accommodate cations (generally an alkali metal) during the redox reactions also ensuring the electroneutrality of the compound. PBAs are suitable materials for host/guest chemistries, displaying high coulombic efficiencies during the insertion/release processes depending on the kind of ion inserted. The high-specificity of the current or voltage applied with the associated electrode potential is the foundation of the preferential electrosorption of ions [16].

PBAs are suitable for the electrochemically switched ion exchange (ESIX) technique, which was recently used for environmental applications, such as the selective removal of radioactive Cs^{+} [14], or separation of Cu^{2+} [17], Ca^{2+} [18] and Ni^{2+} [19]. Each PBA shows different characteristic by changing metal sites (M = transition metal) in the lattice [20], particularly, the capability to intercalate a specific cation. In this context, because their distinctive electrochemical signature and unique structure, PBAs could be potentially considered excellent candidates for the uptake/release of REEs, and the first example has been proposed [21].

Rare earth elements (REEs) have been acquired importance because of their growing applications both in traditional and high-tech industries [22,23]. Their global demand and consumption have been rapidly increasing with the concomitant development of technological devices. The difficult mineral extraction coupled to the limited supplies and their specific location in some areas, lead to the necessity of innovative recovery processes [24].

In this paper, electrodeposited films of CuHCF and NiHCF were adopted for the study of the REEs insertion and release processes, by using an electrochemically-driven one for their recovery. Not only the quantification of the amount of inserted REEs is highlighted but also a study of the kinetic behaviour during the insertion/release process is revealed, by using a chemometric approach of the CVs data.

* Corresponding author.
E-mail address: marco.giorgetti@unibo.it (M. Giorgetti).

https://doi.org/10.1016/j.jelechem.2023.117791
Received 18 June 2023; Received in revised form 24 August 2023; Accepted 10 September 2023
Available online 12 September 2023

2. Materials and methods

2.1. Chemicals

All chemicals were reagent grade from Sigma-Aldrich ($NiCl_2$, Ni $(NO_3)_2$, $K_3Fe(CN)_6$, $Er(NO_3)_3$), Alfa-Aesar ($Gd(NO_3)_3$, $La(NO_3)_3$, Dy $(NO_3)_3$), Merck (KNO_3) and Acros $(Cu(NO)_3)_2$. All experiments have been performed in air, at room temperature, and with bi-deionized water.

2.2. Apparatus

Electrochemical measurements were performed by using a Model 660c (CH Instruments) electrochemical workstation and a standard three-electrode electrochemical glass cell (10 mL). The substrate material of working electrode was glassy carbon GC (diameter ≈ 3 mm) or graphite foil GF (0.10 mm thick, 99.9%, Goodfellow), and a Pt counter electrode was used. All potentials were recorded vs. Ag/AgCl in saturated KCl. The glassy carbon (GC) electrode was polished with a 0.05 μm alumina slurry on a cloth and then rinsed with water.

2.3. Preparation of NiHCF-modified electrodes

NiHCF film was deposited from a solution that contains $1.0{\cdot}10^{-3}$ M $NiCl_2 \cdot 6H_2O$, $1.0{\cdot}10^{-3}$ M $K_3Fe(CN)_6$, and 1.0 M KNO_3 as supporting electrolyte at native pH, through scan between 1.0 V and 0.0 V [9].

2.4. Preparation of CuHCF-modified electrodes

The electrodeposition was carried out at −0.80 V using a solution of 0.05 M $Cu(NO_3)_2$ and 0.1 M KNO_3 as supporting electrolyte for 20 s, then the electrode was rinsed and soaked in $1.0{\cdot}10^{-3}$ M $K_3Fe(CN)_6$ and 0.1 M KNO_3 for 300 s at + 0.6 V. This method was chosen as it appears more suitable for multivalent ion intercalation [8], also ensuring a very good chemical stability.

2.5. Preparation of NiHCF powders

Nickel-hexacyanoferrate powders were synthesized by a simple co-precipitation method and enriched by 1 M $Dy(NO_3)_3$ as already reported [9].

2.6. Electrochemical procedure

The electrochemical behavior in presence of different rare earth cations ($Er(NO_3)_3$, $Gd(NO_3)_3$, $La(NO_3)_3$, $Dy(NO_3)_3$) was investigated by recording CVs in various supporting electrolytes following the protocol: firstly, a CV (10 cycles) was recorded in a KNO_3 0.1 M (solution A), then, other 10 cycles were recorded in a mixture REEs cations 0.1 M (solution B), finally, last 10 cycles scans were repeated in 0.1 M KNO_3 (solution C). This procedure was repeated three times (step1, step2, step3) using the same cell solution, in order to highlight the kinetic behavior.

2.7. MP-AES Analysis

MP-AES analysis was performed on an Agilent 4100 instrument. The Agilent MP Expert software was used to automatically subtract the background signal from the analytical signal. The detailed MP-AES operating conditions are showed in Table S1.

The calibration standards were prepared in the range of 5–5000 ppb using a multielement standard solution in a matrix of 5% HNO_3. The wavelengths used are displayed in Table S2.

2.8. XAS data collection and analysis

X-Ray Absorption experiments were performed at synchrotron Elettra in Basovizza (Italy) at the XAFS beam line [25]. The storage ring operated at 2.0 GeV in top-up mode with a typical current of 300 mA. XAS data were collected at Fe and Ni K-edges and Dy L3-edge in transmission mode using ionization chambers filled with a mixture of Ar, N_2, and He to have 10%, 70%, and 95% of absorption in the I0, I1, and I2 chambers, respectively. X-Ray absorption spectroscopy spectra were deglitched, calibrated, and normalized. The pre-edge background was removed by subtraction of a linear function extrapolated from the pre-edge region, and the XANES spectra were normalized at the unity by extrapolation of the atomic background. The EXAFS analysis was performed by using the GNXAS package [26] that considers Multiple Scattering (MS) theory. More details are available as SI.

2.9. Chemometric analysis

The chemometric analysis was carried out by the EFA Multivariate Curve Resolution (MCR) technique using the Unscrambler X version 10.2, 2009–2012, CAMO softwares and Matlab by TheMathWorks Inc. 1984–2020 with MCR-ALS 2.0 toolbox [27]. The procedure involves a voltammograms sequence: 30 cycles in KNO_3, 30 cycles in REE mixture (uptake REE), 30 cycles in KNO_3, 30 cycles in REE mixture (uptake REE), 30 cycles in KNO_3, again 30 cycles in a KNO_3 clean solution. 180 cycles in KNO_3 were recorded as background. Even though the first REEs intercalation (step 1) caused a reduction in charge capacity, the next exchange processes which account for 160 cycles, led to a 50% retention in charge capacity.

3. Results and discussion

In this section, we present at first the electrochemical behaviour of the electrodeposited PBAs, elucidating their REE insertion/release capability and as well as proving the structural site where RE ions are located. Then, we delve into the quantification of the recovered REE. This is followed by a chemometric examination applied to the CV data, which provides the kinetic details of the REE insertion/release process. Cyclic voltammetry is the most common electrochemical technique employed in the investigation of PBAs [8–10]. This choice is motivated by its ability to simulate the reduction and oxidation reaction of $Fe^{II/III}$ and it also offers a fast diagnosis of the intercalation process by the cycles. Furthermore, for the adopted protocol, including the chemometric studied, CV was needed to assess the kinetic behaviour of the system, complemented by the application of chemometric techniques.

To the side of the REE chemistry, four specific rare earth elements (dysprosium, lanthanum, erbium, and gadolinium) were chosen. This selection is based on the classification of REEs according to their chemical properties, resulting in three distinct groups: heavy (HREE, Dy to Lu), middle (MREE, Sm, Gd, Tb, Eu) and light (LREE, La, Ce, Pr, Nd) [28]. Therefore, we are proposing a study focused on the distinguishing characteristics, particularly the variation in ionic radii size, between the light rare earth elements (LREE) and heavy rare earth elements (HREE).

3.1. Electrochemical behaviour of NiHCF and CuHCF as a host material

To elucidate the distinctive morphological features observed in the cyclic voltammetry (CV) of NiHCF and CuHCF, a brief description is needed. NiHCF CV shows a shoulder due to the two different specie: K-rich and Ni-rich [29]. On the other hand, the second reduction peak showed in CuHCF CV is related to the Cu(II)/Cu(I) reduction process [30]. The electrodeposition of NiHCF and CuHCF on GCE was carried out following a precise protocol detailed in the SI. This approach enabled the investigation of the CuHCF and NiHCF electrochemical host capabilities concerning various RE cations. This protocol permitted the assessment of the K^+ replacement with the tested RE cations and, in the last step, to check the process reversibility. This procedure was applied to several rare earth elements cations, namely, La^{3+}, Gd^{3+}, Dy^{3+} and Er^{3+}.

In view of the previous report [29], the following approximate formulas can be assigned to two predominant forms of electrodeposited NiHCF films: $K_2Ni^{II}[Fe^{II}(CN)_6]$ and $KNi^{II}_{1.5}[Fe^{II}(CN)_6]$. Ciabocco *et al.* [9] showed the NiHCF capability to intercalate easily trivalent cations as well as monovalent cations. Furthermore, CuHCF was electrodeposited, being $KCu^{II}[Fe^{III}(CN)_6]_2$ and $K_2Cu^{II}[Fe^{II}(CN)_6]_2$ the two phases related to the two peaks at ca. + 0.8 V. Similarly, CuHCF was studied as ionic exchange framework for mono, di-valent and trivalent cations [6,8,19,20], supported by wide characterization studies [8,31], which highlight no substitution in the lattice during the intercalation. Hence, both of them can be used as a membrane for the reversible ion intercalation.

Both PBAs shows a well-defined shape during CVs: Fig. 1B shows CV scans of CuHCF recorded in potassium nitrate before (black line) and after (red line), the test in dysprosium nitrate (blue line). The complete overlap of the CVs recorded in K^+ is striking and underlines the reversibility of the process. The voltammogram recorded in $Dy(NO_3)_3$, similar to the other REE tested (Fig. 1D), reaches a potential stability in 4 cycles, which is slower compared to the K^+ electrolyte.

Fig. 1A shows the reversible process toward to the erbium nitrate intercalation/release in NiHCF film. The first 10 cycles recorded in KNO_3 (black line) are almost coincident with the last (red line) recorded after performing 10 cycles in a solution containing Er^{3+} cations (blue line); thus, the alignment unequivocally confirms the perfect cation exchange reversibility. From Fig. 1A it seems that the insertion of erbium occurs faster than the potassium uptake, as observed by the relatively different peak potential shift in their respective CVs. This attitude might highlight the different kinetic control between mono-charge and tri-charge cations during the intercalation/deintercalation. For this reason, the kinetic behaviour was investigated in depth using a chemometric approach, detailed in Section 3. Generally speaking, a perfect reversibility is observed with all the investigated cations.

Furthermore, in order to check the accommodation of REEs into a specific crystalline site, a XAS analysis (Fig. 2) was carried out on NiHCF powders obtained by the coprecipitation methods, enriched with Dy salt as a representative example.

By using the strong selectivity of the XAS for the atomic species, all the three metals environment can be checked out and revealed, namely the Fe, Ni and the Dy. As expected, a six orthogonal -Fe-CN-Ni- structural framework is observed, where Fe and Ni alternatively occupy vertex position of a cubic network. This can be seen from the typical XANES curves taken at the Fe and Ni K-edges of Fig. 2 [32,33] and also by the EXAFS analysis reported in the SI. Specifically, the six Fe-C, the C ≡ N, and the Ni-N distances are 1.903(6), 1.175(10) and 1.95(3) Å, respectively. Of more importance is the determination of the Dy coordination site. The EXAFS analysis has indicated a dysprosium first-shell coordination site as formed by of 2.2(4) oxygen atoms at 2.30(2) Å, plus a second interaction due to carbon or nitrogen at 3.61 Å and finally a Dy- -Fe(Ni) long interaction at 4.35 Å. The full picture indicates unambiguously that the Dy occupies intercalation site at the centre of the cube (Fig. 2, panel F), in position that are frequently called “zeolitic position” [34], allowing the easy intercalation /release of guest ions in metal hexacyanoferrates.

Fig. 3 displays the comparison of the CV curve of NiHCF powder and of the electrodeposited one, which we have further used in this paper, showing the same CV shape. This feature, together with the electrochemical reversibility data (Fig. 1) and the XAS data, excludes any possible Ni or Fe substitution in the hexacyanoferrate structural network

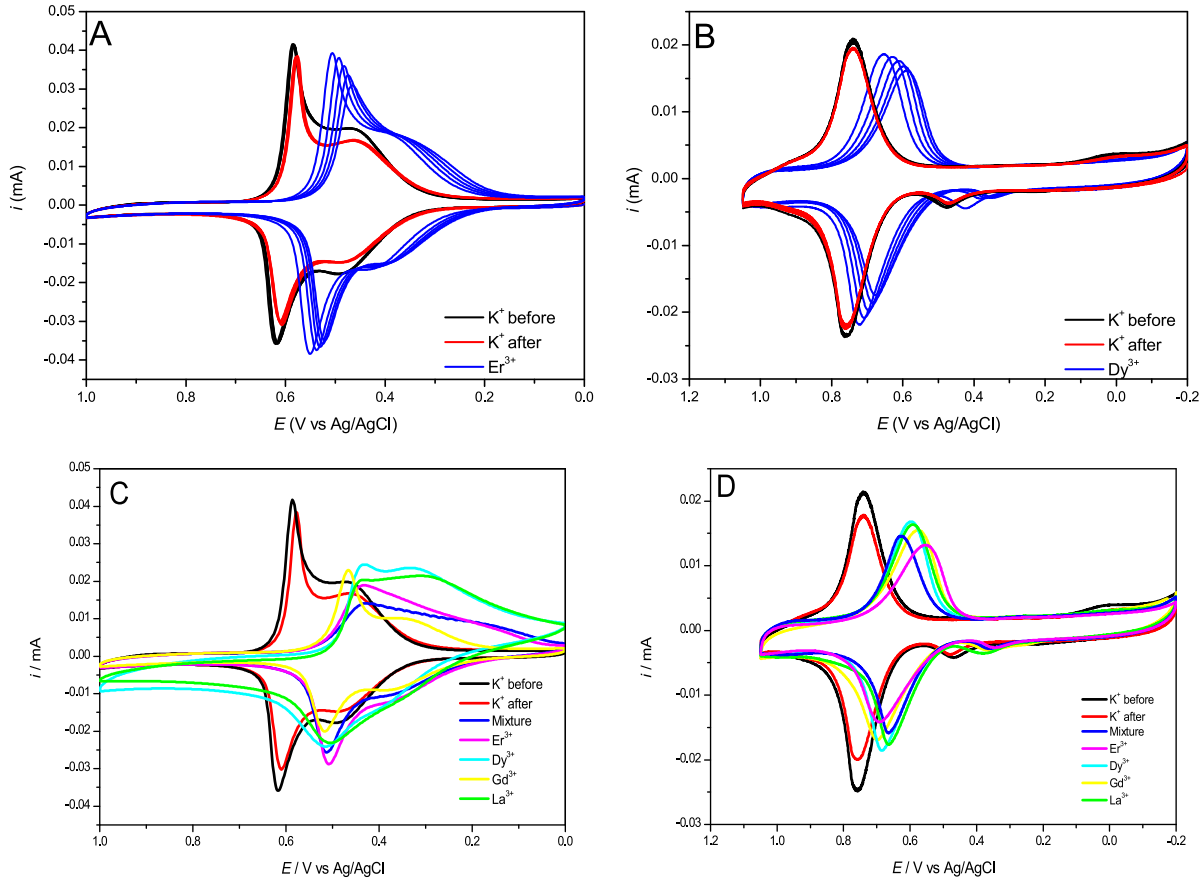

Fig. 1. CVs at 0.1 V s^{-1} of GCE modified with A) NiHCF film in 0.1 M KNO_3 and 0.1 M $Er(NO_3)_3$ solutions at native pH; B) CuHCF film in 0.1 M KNO_3 and 0.1 M $Dy(NO_3)_3$ solutions at native pH; C) NiHCF in 0.1 M KNO_3, 0.1 M $RE(NO_3)_3$ and D) CuHCF thin film in 0.1 M KNO_3, 0.1 M $RE(NO_3)_3$ (RE = La, Dy, Gd, Er), solutions and in mixture containing rare earth cations at native pH.

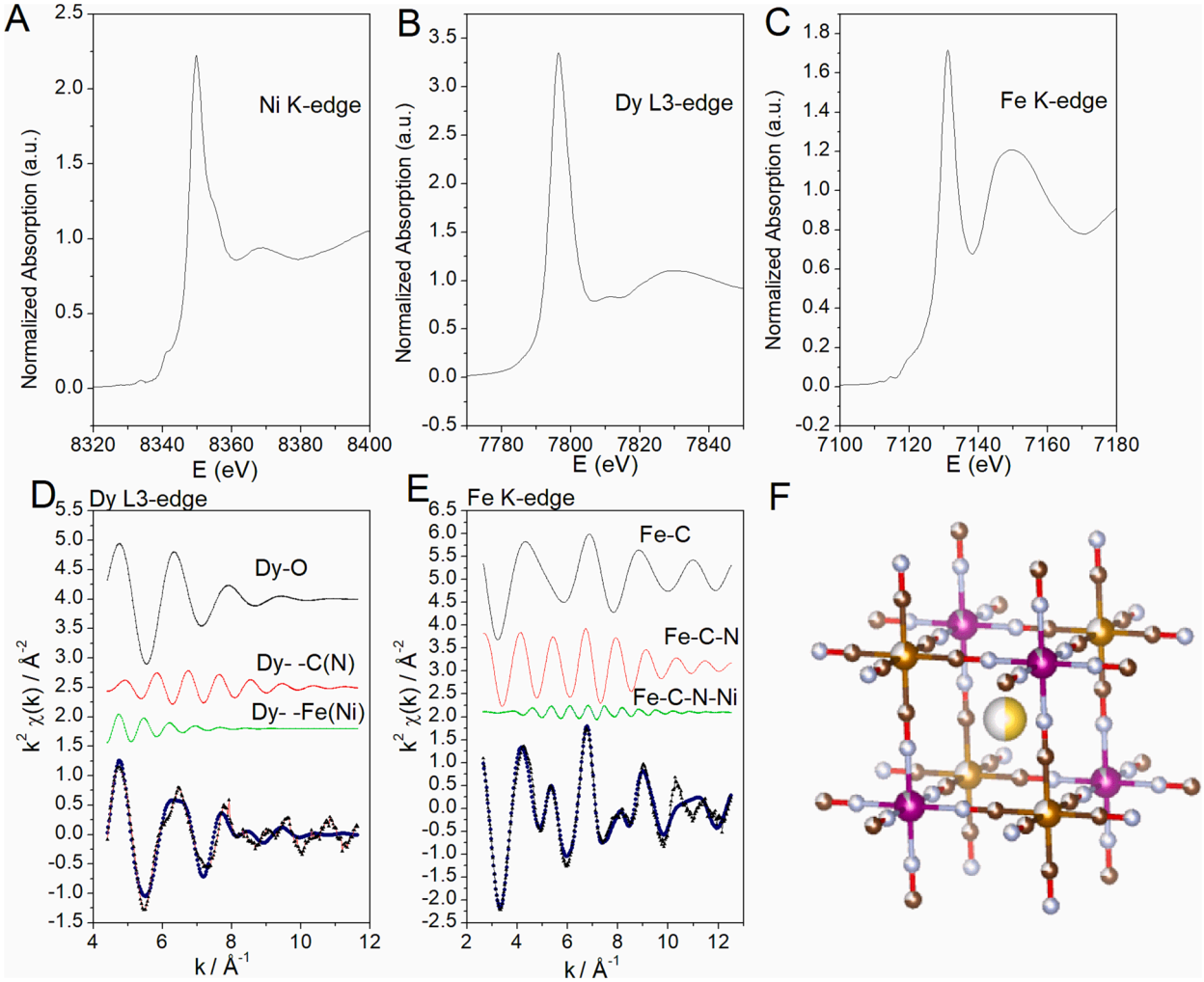

Fig. 2. XAS analysis of $DyNiFe(CN)_6$ material. XANES spectra at Ni K-edge (panel A), L3-edge of Dy (panel B) and Fe K-edge (panel C). EXAFS analysis at L3-edge of Dy (panel D) and Fe K-edge (panel E) in terms of individual contribution to the total EXAFS signals, and crystallographic structure (panel F). The Dy atom is located at the cube centre in yellow (zeolytic position). (For interpretation of the references to colour in this figure legend, the reader is referred to the web version of this article.)

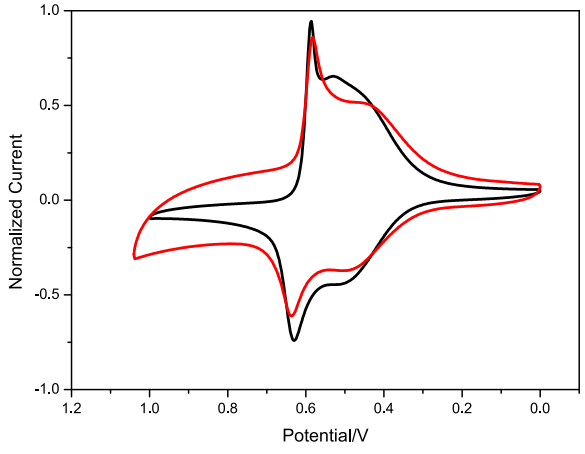

Fig. 3. CVs overlay of NiHCF-powders (black line) and NiHCF-film (red line) in KNO_3 0.1 M at 0.1 V s^{-1} vs Ag/AgCl. (For interpretation of the references to colour in this figure legend, the reader is referred to the web version of this article.)

as a consequence of the metal ion insertion. Generally, during the CV scans of the investigated rare earth cations, we never observed a partial substitution of Ni, coordinated to the N atom, by the guest cations. A possible partial substitution in the case of PB was suggested [35] in one case, where the *N*-coordinated iron was partially replaced by Ni^{2+} or Cd^{2+} when a cycling polarisation step was performed in solutions containing these cations.

The dependence of CVs upon the concentration has been further studied for each rare-earth cation in the $1.0 - 1.0 \times 10^{-2}$ M range in order to assess the role of the rare earth cation in the electrochemical process. The redox mechanism involves the rare earth cations insertion during reduction and its release during oxidation, according to the following reactions:

$$Ni_{1.5}\left[Fe^{III}(CN)_6\right] + 1/3A^{3+} + e^- \rightleftarrows A_{1/3}\left[Ni_{1.5}Fe^{II}(CN)_6\right] \quad (1)$$

$$Cu_3\left[Fe^{III}(CN)_6\right]_2 + 1/3A^{3+} + e^- \rightleftarrows A_{1/3}\left[Cu_3Fe^{II}(CN)_6\right]_2 \quad (2)$$

The Nernst equation for reactions (1) and (2) reads (in volts):

$$E = E_0 + \left(\frac{0.059}{3}\log\left[A^{3+}\right]\right) \quad (3)$$

where A is one of the rare earth ions between erbium, lanthanum, dysprosium, or gadolinium. All the experiments, therefore, confirm the

insertion/de-insertion mechanism of the tested REEs as proved by the Nernstian slope values very close to the theoretical one of 19 mV, expected for trivalent cations. The related data were showed in SI. This phenomenon arises as a consequence of the zeolitic structure of the PBA characterized by open channels whose chemical-physical characteristics constitute the driving force for ion discrimination. Furthermore, the nature and the size of the ion play a key role in influencing their insertion into the structure.

To fully check the electrochemical behaviour of the both electrodeposited PBAs, several CVs were recorded in 0.1 M $La(NO_3)_3$, $Gd(NO_3)_3$, $Dy(NO_3)_3$ and $Er(NO_3)_3$ solutions at 0.1 V s^{-1} and in a mixture containing all the investigated rare earth elements (the last cycle is reported in Fig. 1C and 1D). Both for CuHCF and NiHCF, no shape modification occurs during the REE insertion, but only a potential shift takes place, as reported for other cations [8,9].

By analysing the peak position, it became evident that we could draw comparisons between the CV of mixed cations and that of a specific cation, regardless the nature of the rare earth cations involved. In most cases, substituting K^+ ions with another cation led to significant alterations in peak shape and position. These shifts in peak potentials can be attributed to either the hydrated cation's radius, as previously observed in other Prussian Blue-type compounds [36] or to the ionic potential (ratio of ionic charge/radius) as reported by [37]. Moreover, the potential shift is also influenced by both the ionic radii and the metal composition of the PBA. Specifically, CuHCF, due to its higher potential, exhibits a greater propensity for the intercalation of hydrated ions when compared to NiHCF [20].

On one hand, the cyclic voltammograms (CVs) of NiHCF (Fig. 1C) demonstrated the excellent reversibility of the process and exhibited the expected potential shift for each tested REE. In addition, the distinctive shape of the CVs hinted at the potential preference of NiHCF for intercalating dysprosium as a preferred REE. On the other hand, the CVs of CuHCF (Fig. 1D) did not exhibit a distinct shape, suggesting the absence of a preferred ion for intercalation. Thus, a further investigation was needed to quantify the ion intercalated.

3.2. MP-AES analysis

In order to quantify the amount of REEs up-taken by PBAs, MP-AES analysis were carried out on an Agilent 4100 instrument. To obtain an adequate quantity to be tested at MP-AES, the protocol was transferred from GC to GF, where an electrode surface area of ~ 1.5 cm^2 was reached (ca 95% increase). Thus, increasing the electroactive area, the quantity of the ion intercalated increased accordingly. In particular, a specific protocol was adopted (Fig. 4), i.e.: three steps were carried out, where each step consists of 10 CV scans recorded in potassium nitrate (solution (A)), 10 CV scans recorded in a REEs mixture (solution (B)), 10 CVs recorded in potassium nitrate again (solution (C)). For each step 1 mL of the solution (C) was examined by MP-AES. The related CV scans were reported in the SI.

Even though several wavelengths were tested (see the SI), the best one was selected: dysprosium (353.171 nm), erbium (390.631 nm), lanthanum (433.374 nm).

An adequate reproducibility and quantifying for gadolinium were not attainable for all of the wavelengths chosen, even though interference were not anticipated [38].

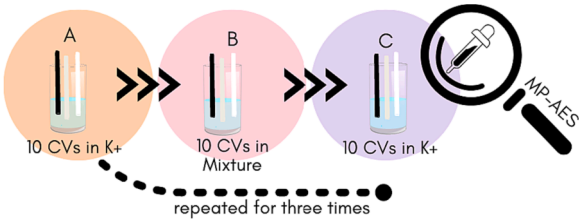

Fig. 4. The schematic procedure followed for the MP-EAS analysis.

The results showed in Table 1 indicate the RE ion concentration in mM (average concentration from two data set) for each protocol step in the mixture and the related calculated selectivity coefficient. The ions amount is comparable for both PBAs. In the case of CuHCF, its REE-intercalation capability is shown in Fig. 5A. Here, the concentration of each REE remains relatively stable during the first two steps and consistently increases in the last step. The high concentration of dysprosium and also to some extent erbium, indicates that CuHCF intercalates preferentially heavier ions even from the first step. Conversely, lanthanum concentration is found to be lower than the others. Kinetically, the quantity of ions progressively increases during each step, therefore ten cycles are needed to uptake roughly the same quantity. Unlike CuHCF, NiHCF shows a different behaviour from a kinetic point of view. The REEs concentration does not follow a linear increase: it is lower at the beginning and becomes very high toward the end. Thus, more than 10 cycles are needed for a stable intercalation. The reason why it occurs, may be due to the rearrangement of the lattice due to the accommodation of cations into the structure during the scans. NiHCF intercalation capability results different from the CuHCF one and the selectivity capacity of each PBA was evaluated by the selectivity coefficient (K), calculated by the Eq. (4), where the C_x is the concentration of one ion and C_{mix} is the total concentration of the REEs mixture in each protocol step [39].

$$K_x = \frac{C_x}{C_{mix}} \tag{4}$$

The interesting feature of CuHCF was its capability to intercalate dysprosium and erbium rather than lanthanum, with a 1:10 ratio during the first two steps but a 1:2 ratio was reached at the end of the procedure. The selectivity coefficient (Fig. 5C) suggests that the dysprosium intercalation occurs easily rather than the lanthanum one, which might be due to the different size: the lanthanum ionic radii is bigger than the other ones, whose size are comparable (Table 2). Instead, during the first two steps the NiHCF shows a particular capability to intercalate dysprosium and erbium, and at the end (Step 3) also lanthanum was intercalated (Fig. 5C), indeed its amount increases.

The distinctive behaviour of the two PBAs towards lanthanum intercalation could be associated to the diverse way to accommodate hydrated, fully dehydrated, or partially- hydrated cations. Indeed, data literature reports that the insertion of hydrated alkali metal ions is easier in CuHCF over NiHCF [16]. In addition, being light rare earth ions nonahydrates, unlike the heavy rare earth ions which are octahydrates (forming anionic complex) in aqueous solution [41], that could be a discerning feature for their intercalation.

Table 1
RE ions concentration evaluation (MP-AES data) during the protocol using NiHCF and CuHCF thin films on Grafoil, and related selectivity coefficient calculated by Eq. (4).

		CuHCF	CuHCF	NiHCF	NiHCF
Protocol Steps	*IONS*	*Concentration (mM)*	*K, Selectivity coefficient*	*Concentration (mM)*	*K, Selectivity coefficient*
1	Dy^{3+}	0,924	0,584	0,746	0,468
2	Dy^{3+}	1,174	0,588	0,697	0,456
3	Dy^{3+}	2,196	0,452	3,224	0,393
1	Er^{3+}	0,527	0,333	0,531	0,333
2	Er^{3+}	0,64	0,321	0,453	0,297
3	Er^{3+}	1,634	0,336	2,539	0,31
1	La^{3+}	0,132	0,083	0,318	0,199
2	La^{3+}	0,181	0,091	0,377	0,247
3	La^{3+}	1,030	0,212	2,434	0,297
1	*Cmix*	1,583		1,595	
2	*Cmix*	1,995		1,527	
3	*Cmix*	4,86		8,197	

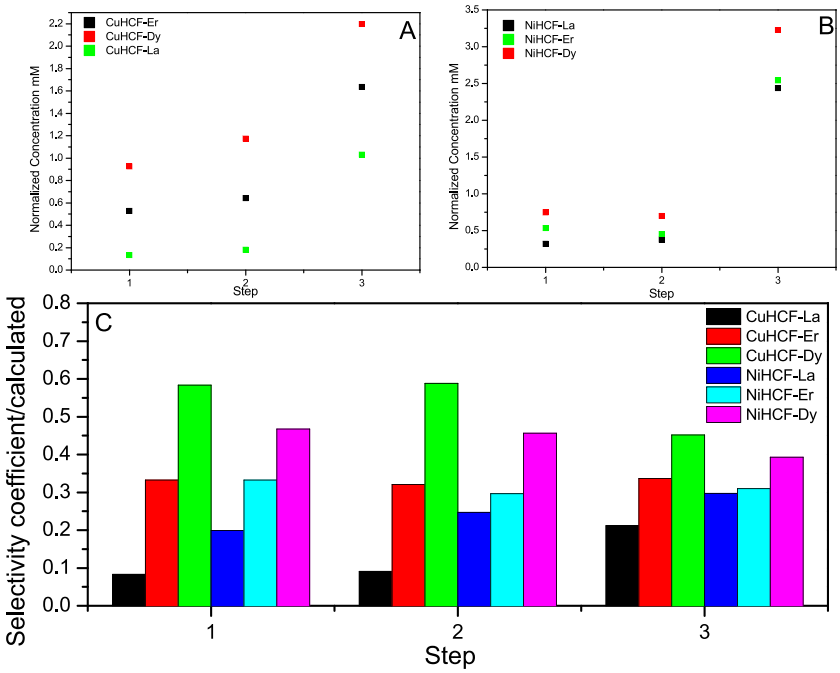

Fig. 5. Concentration of REEs A) CuHCF B) NiHCF - data obtained by MP-AES. C) Selectivity coefficient calculated for each REE on CuHCF and NiHCF.

Table 2
Ionic radii and hydration enthalpy values of dysprosium, lanthanum and erbium [40].

cations	radius (Å)	ΔH_{hyd} (KJ·mol^{-1})
La^{3+}	1.06	−3285
Dy^{3+}	0.91	−3577
Er^{3+}	0.89	−3621

3.3. Chemometry: Multivariate curve resolution method

The different NiHCF profile obtained by the CV data were examined from a kinetic point of view, as MP-AES data suggested a non-linear kinetic profile. This approach uses the multivariate curve resolution-alternating least squares (MCR-ALS) method, which is a method for analysing multivariate data affected by an evolutionary change, applied on different datasets [42,43]. MCR-ALS method was adopted because it enables the detection of the number of species and the evolution of their concentration during a defined evolutionary process [44]. The goal of the MCR is to decompose the data matrix, **X**, in a column profiles of concentration matrix, **C**, by a row profile of the components (voltammograms) matrix, **V**, of the analysed mixture: $\mathbf{X} = \mathbf{C}\mathbf{V}^t$. The hypothesis is that the rank of a data matrix corresponds to the number of the true substances in the mixture. Principal Component Analysis (PCA) is generally used to find the rank of a data matrix and decompose it into the product of two abstract factor matrices. EFA (Evolving factor analysis) applies this property of PCA analysing submatrices of **X** of increasing dimension; in this way EFA permits to define the field of existence of the single species, that is a first approximation of matrix **C**. Using this approximation of the concentration profiles and the data matrix **X,** it is possible to compute the matrix **V** by the least squares method. Iterating with some constraints it is possible to refine by Alternating Least Squares (ALS) the decomposition of matrix **X**. The REEs extraction/separation procedure is based on an exchange process, in which K^+ was exchanged by REE and afterward a REE was released, allowing the reinsertion of K^+. A voltammograms sequence of NiHCF thin film on GCE was carried out using the protocol described in the experimental section.

We adopted several constraints for the MCR-ALS analysis: firstly, the closure condition, that provide the mass balance conservation, and additionally the non-negativity of the concentration profiles. The application of EFA technique allows to define the presence of several species and their evolution (in terms of concentration). By adjusting one or more parameters, providing the mass balance conservation (closure condition). For our aim, this closure condition ensures that the total charge remains constant, signifying that the same amount of electrode material is involved in reactions throughout the recorded cycles. Fig. 6B shows 180 cycles of the NiHCF modified electrode in 0.1 M KNO_3 solution: the voltammogram shape changes with the increasing of the cycles number. Indeed, if on one hand the cathodic peak intensity at ca + 0.55 V decreases, on the other hand the peak at ca. + 0.40 V increases. Furthermore, the charge decrement over the time is due to the loss of the electrode material.

In order to mitigate the possible loss of electroactive material and therefore ensuring the closure conditions, the voltammograms were normalized by keeping the charge constant. For clarity, only the cathodic process of the voltammograms was presented. (Fig. 6D).

The presence of a clear isosbestic point (at ca. 0.45 V) in the cathodic span, as show the inset of Fig. 6B, is due to the morphological evolution of the voltammograms indicates the progressive changing from the K-rich-specie to the Ni-one [29]. This particular characteristic is confirmed by the calculated concentration obtained from the MCR-ALS analysis (Fig. 6A). Then, the 180 cycles of REEs extraction procedure were analysed. In Fig. 6C the overlapped and charge normalized cathodic CVs (180 cycles in total) were reported.

The gradual increase in the number of cycles induces a progressive transformation in the peak morphology, mirroring the behaviour observed in NiHCF with KNO_3, as discussed earlier. The CVs recorded in the mixture of REEs, after the first cycles, the morphology of the voltammograms remains constant. The concentration profiles reported in Fig. 6C were calculated by EFA, by fixing three species: K-rich-NiHCF, Ni-rich-NiHCF, the NiHCF containing REE. To this elaboration data was overlapped the curves obtained from the background elaboration (dot curves). A close inspection of Fig. 6C highlights the six different steps examined:

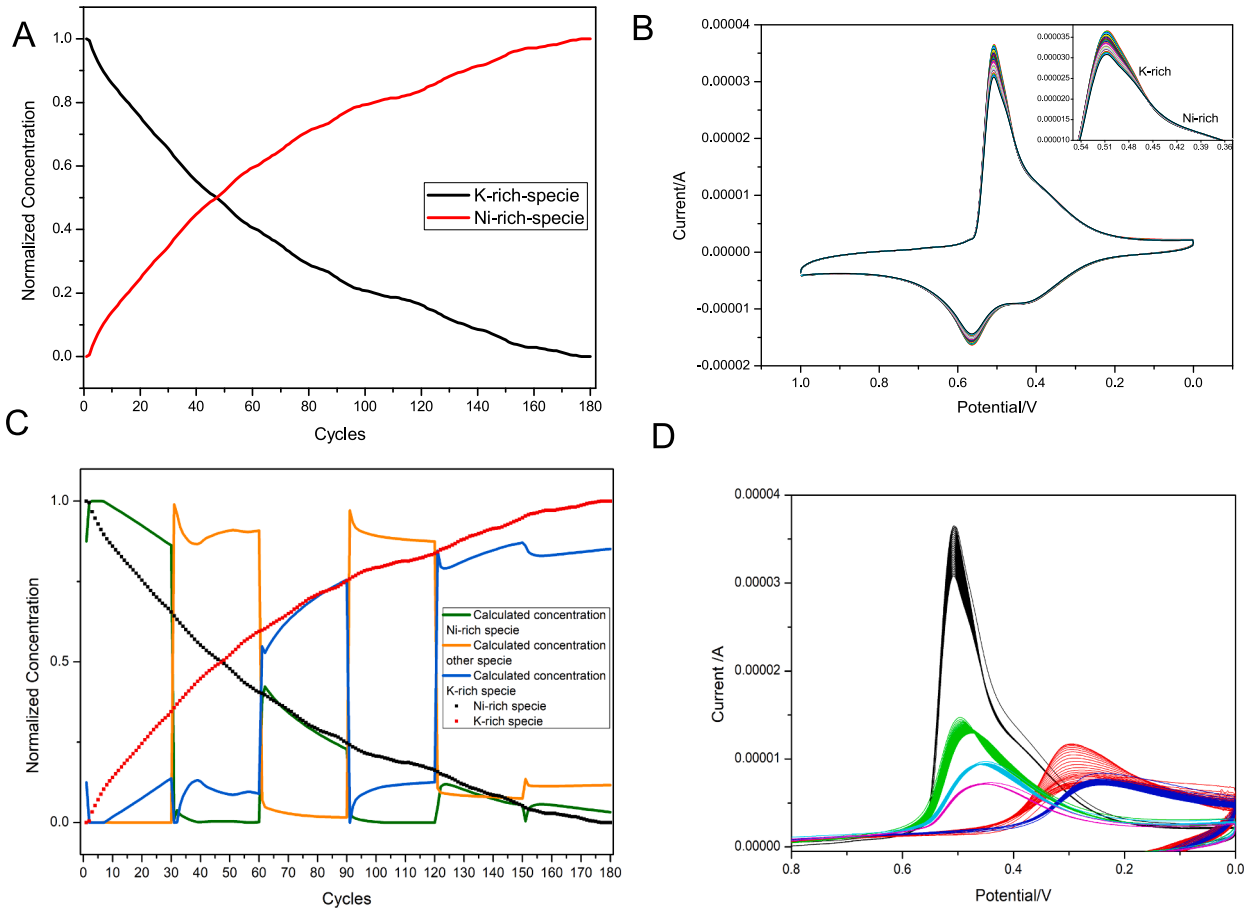

Fig. 6. A) Calculated concentrations profiles of Ni-rich-specie (red) and K-rich-specie (black). B) CVs of NiHCF film. 180 cycles recorded in KNO_3 0.1 M on GCE. Inset: cathodic voltammograms overlapping cycle 1–180. C) Concentration profiles calculated fixing 3 species. The dot curves show the overlapping of the K-rich-NiHCF (red), Ni-rich-NiHCF (black) obtained by the 180 cycles in KNO_3 elaboration. The green, orange and blue lines show the three species calculated concentration from MCR-ALS. D) Overlapped cathodic voltammograms, charge normalized. The six phases are marked by different colours. CVs of NiHCF recorded in: KNO_3 (1st step) - black line, Mixture (2nd step) - red line, KNO_3 (3rd step)- green line, Mixture (4th step)- blue line, KNO_3 (5th step)- cyan line, clean-KNO_3 (6th step) - magenta line. (For interpretation of the references to colour in this figure legend, the reader is referred to the web version of this article.)

- 1st Step (cycles 1–30) in KNO_3: in the first 30 cycles only two species are discernible: the K-rich-specie (blue line- curve 1), the predominant specie, and Ni-rich specie (green line - curve 2).
- 2nd Step (cycles 31–60) in REEs mixture: starting from the 31st cycle a new specie (orange line- curve 3) appears while, concurrently, the curves 1 and 2 almost completely disappear. The curve 3 shows some fluctuation before reaching a steady state.
- 3rd Step (cycles 61–90) in KNO_3: here, the curve 3 immediately decays to zero, suggesting that only two cycles required for the REEs releasing and the re-uptake of K^+. The intensity of curves 1 and 2 are inverted.
- 4th Step (cycles 91–120) in REEs mixture: the situation is analogous to the one observed in the 3rd step.
- 5th Step (cycles 121–150) in KNO_3: the curve 3 immediately decline to zero, therefore the releasing of REEs occurs. The curve 1 still decreases and the curve 2 still increases.
- 6th Step (cycles 161–180) in KNO_3: here, a stabilization of the curve 1 (decreasing) and curve 2 (increasing) occurs.

It worth noting that the evolution of the curves 1 (blue) and 2 (green) matches with the dot curves (black and red dot curves), obtained by the 180 cycles recorded in KNO_3, showing a perfect overlapping of the dot curves. Thus, the release of REEs occurs faster than their uptake. The delay in the REEs uptake can be related to its accommodation into the hexacyanoferrate lattice, which may depend on the size of the REE. This explains that the different starting behaviour of dysprosium/erbium and lanthanum is probably due to the larger ionic radii [45] of lanthanum, which is less easily intercalated into the structure, as already evidenced from the MP-AES data.

4. Conclusions

In summary, this paper focuses on the electrochemical performance of NiHCF and CuHCF thin films as hosts for the rare earth elements. Both PBAs exhibit reversible intercalation of RE ions without any metal substitution in the crystalline site, as confirmed by results obtained by applying the high selectivity of the X-ray Absorption Spectroscopy (XAS) probe.

The quantification of the recovered REEs and the variation of individual ion concentrations over time were determined using MP-AES analysis. The experiments revealed that NiHCF initially had a preference for intercalating smaller ions (Dy^{3+} and Er^{3+}), then an indiscriminate intercalation have occurred. The amount of intercalated RE cations increased nonlinearly over the cycles.

In contrast, CuHCF showed an easier intercalation of the heavy rare earth elements rather than the light ones and their amount increased linearly over time. The peculiar NiHCF kinetic behaviour, as revealed by the MP-AES data further explored through MCR-ALS analysis of their respective CVs. This analysis confirmed both the presence of another species during the redox process (REE over the Ni-rich and K-rich

species), and the slow REE uptake, as already anticipated by the CVs. Additionally, the chemometric analysis emphasized that the intercalation of RE ions occurs more gradually than their release, likely due to the time needed for the lattice accommodation during the redox process.

Overall, these findings provide a relevant step forward for the identification of methods for the REEs enrichment and recovery from a multicomponent matrix. The electrochemical approach here proposed is proven to be effective.

CRediT authorship contribution statement

Rosalinda Sciacca: Conceptualization, Writing – original draft, Writing – review & editing. **Mario Berrettoni:** Conceptualization, Writing – review & editing. **Paolo Conti:** Conceptualization, Writing – review & editing. **Marco Giorgetti:** Conceptualization, Writing – original draft, Writing – review & editing.

Declaration of Competing Interest

The authors declare that they have no known competing financial interests or personal relationships that could have appeared to influence the work reported in this paper.

Acknowledgements

RFO funding from the university of Bologna is kindly acknowledged. XAS measurements at ELETTRA were supported by CERIC project #20222183 (M.G. as PI).

Appendix A. Supplementary data

Supplementary data to this article can be found online at https://doi.org/10.1016/j.jelechem.2023.117791.

References

[1] N.R. de Tacconi, K. Rajeshwar, R.O. Lezna, Metal hexacyanoferrates: electrosynthesis, in situ characterization, and applications, Chemistry of Materials 15 (2003) 3046–3062, https://doi.org/10.1021/cm0341540.
[2] M. Li, R. Sciacca, M. Maisuradze, G. Aquilanti, J. Plaisier, M. Berrettoni, M. Giorgetti, Electrochemical performance of manganese hexacyanoferrate cathode material in aqueous Zn-ion battery, Electrochimica Acta 400 (2021) 139414.
[3] S. Qiu, Y. Xu, X. Wu, X. Ji, Prussian blue analogues as electrodes for aqueous monovalent ion batteries, Electrochem. Energy Rev. 5 (2022) 242–262, https://doi.org/10.1007/s41918-020-00088-x.
[4] H. Düssel, A. Dostal, F. Scholz, Hexacyanoferrate-based composite ion-sensitive electrodes for voltammetry, Fresenius' Journal of Analytical Chemistry 355 (1996) 21–28, https://doi.org/10.1007/s0021663550021.
[5] M.A. Malik, P.J. Kulesza, R. Marassi, F. Nobili, K. Miecznikowski, S. Zamponi, Countercation intercalation and kinetics of charge transport during redox reactions of nickel hexacyanoferrate, Electrochimica Acta. 49 (2004) 4253–4258, https://doi.org/10.1016/j.electacta.2004.04.021.
[6] L.D. Reed, S.N. Ortiz, M. Xiong, E.J. Menke, A rechargeable aluminum-ion battery utilizing a copper hexacyanoferrate cathode in an organic electrolyte, Chemical Communications 51 (2015) 14397–14400, https://doi.org/10.1039/C5CC06053B.
[7] R.Y. Wang, B. Shyam, K.H. Stone, J.N. Weker, M. Pasta, H.-W. Lee, M.F. Toney, Y. Cui, Reversible multivalent (monovalent, divalent, trivalent) ion insertion in open framework materials, Advanced Energy Materials 5 (2015) 1401869, https://doi.org/10.1002/aenm.201401869.
[8] M. Ventura, A. Mullaliu, D.E. Ciurduc, S. Zappoli, G. Giuli, D. Tonti, E. Enciso, M. Giorgetti, Thin layer films of copper hexacyanoferrate: Structure identification and analytical applications, Journal of Electroanalytical Chemistry. 827 (2018) 10–20, https://doi.org/10.1016/j.jelechem.2018.08.044.
[9] M. Ciabocco, M. Berrettoni, S. Zamponi, R. Spinosi, P. Conti, An overview on the facile and reversible cations intercalation in nickel-hexacyanoferrate open framework, International Journal of Electrochemical Science 13 (6) (2018) 5535–5551.
[10] R. Sciacca, S. Zamponi, M. Berrettoni, M. Giorgetti, Stable films of zinc-hexacyanoferrate: electrochemistry and ion insertion capabilities, Journal of Solid State Electrochemistry 26 (1) (2022) 63–72.
[11] M. Giorgetti, E. Scavetta, M. Berrettoni, D. Tonelli, Nickel hexacyanoferrate membrane as a coated wire cation-selective electrode, The Analyst 126 (2001) 2168–2171, https://doi.org/10.1039/b107034g.
[12] S.D. Rassat, J.H. Sukamto, R.J. Orth, M.A. Lilga, R.T. Hallen, Development of an electrically switched ion exchange process for selective ion separations, Separation and Purification Technology. 15 (1999) 207–222, https://doi.org/10.1016/S1383-5866(98)00102-6.
[13] M. Pyrasch, A. Toutianoush, W. Jin, J. Schnepf, B. Tieke, Self-assembled films of prussian blue and analogues: optical and electrochemical properties and application as ion-sieving membranes, Chemistry of Materials 15 (2003) 245–254, https://doi.org/10.1021/cm021230a.
[14] R. Chen, H. Tanaka, T. Kawamoto, M. Asai, C. Fukushima, H. Na, M. Kurihara, M. Watanabe, M. Arisaka, T. Nankawa, Selective removal of cesium ions from wastewater using copper hexacyanoferrate nanofilms in an electrochemical system, Electrochimica Acta. 87 (2013) 119–125, https://doi.org/10.1016/j.electacta.2012.08.124.
[15] R. Chen, H. Tanaka, T. Kawamoto, M. Asai, C. Fukushima, M. Kurihara, M. Ishizaki, M. Watanabe, M. Arisaka, T. Nankawa, Thermodynamics and mechanism studies on electrochemical removal of cesium ions from aqueous solution using a nanoparticle film of copper hexacyanoferrate, ACS Applied Materials & Interfaces 5 (2013) 12984–12990, https://doi.org/10.1021/am403748b.
[16] J.G. Gamaethiralalage, K. Singh, S. Sahin, J. Yoon, M. Elimelech, M.E. Suss, P. Liang, P.M. Biesheuvel, R.L. Zornitta, L.C.P.M. de Smet, Recent advances in ion selectivity with capacitive deionization, Energy and Environmental Science 14 (2021) 1095–1120, https://doi.org/10.1039/D0EE03145C.
[17] F. Gao, X. Du, X. Hao, S. Li, X. An, M. Liu, N. Han, T. Wang, G. Guan, An electrochemically-switched BPEI-CQD/PPy/PSS membrane for selective separation of dilute copper ions from wastewater, Chemical Engineering Journal. 328 (2017) 293–303, https://doi.org/10.1016/j.cej.2017.06.177.
[18] C. Weidlich, K.-M. Mangold, Electrochemically switchable polypyrrole coated membranes, Electrochimica Acta. 56 (2011) 3481–3484, https://doi.org/10.1016/j.electacta.2010.11.065.
[19] Z. Wang, Y. Feng, X. Hao, W. Huang, X. Feng, A novel potential-responsive ion exchange film system for heavy metal removal, Journal of Materials Chemistry A. 2 (2014) 10263–10272, https://doi.org/10.1039/C4TA00782D.
[20] M. Asai, A. Takahashi, K. Tajima, H. Tanaka, M. Ishizaki, M. Kurihara, T. Kawamoto, Effects of the variation of metal substitution and electrolyte on the electrochemical reaction of metal hexacyanoferrates, RSC Advances 8 (2018) 37356–37364, https://doi.org/10.1039/C8RA08091G.
[21] M. Berrettoni, A. Mullaliu, M. Giorgetti, Metal Hexacyanoferrate Absorbents for Heavy Metal Removal, in: Inamuddin, M.I. Ahamed, E. Lichtfouse, A.M. Asiri (Eds.), Green Adsorbents to Remove Metals, Dyes and Boron from Polluted Water, Springer International Publishing, Cham, 2021: pp. 171–194. https://doi.org/10.1007/978-3-030-47400-3_7.
[22] M.A. Alam, L. Zuga, M.G. Pecht, Economics of rare earth elements in ceramic capacitors, Ceramics International. 38 (2012) 6091–6098, https://doi.org/10.1016/j.ceramint.2012.05.068.
[23] X. Du, T.E. Graedel, Global In-Use Stocks of the Rare Earth Elements: A First Estimate, Environmental Science & Technology 45 (2011) 4096–4101, https://doi.org/10.1021/es102836s.
[24] Q. Tan, J. Li, Rare earth metal recovery from typical e-waste, in: V. Goodship, A. Stevels, J. Huisman (Eds.), Waste Electrical and Electronic Equipment (WEEE) Handbook, (Second Edition),, Woodhead Publishing, 2019, pp. 393–421, https://doi.org/10.1016/B978-0-08-102158-3.00015-X.
[25] G. Aquilanti, M. Giorgetti, R. Dominko, L. Stievano, I. Arčon, N. Novello, L. Olivi, Operando characterization of batteries using x-ray absorption spectroscopy: advances at the beamline XAFS at synchrotron Elettra, Journal of Physics D: Applied Physics 50 (7) (2017) 074001.
[26] A. Filipponi, null Di Cicco A,, X-ray-absorption spectroscopy and n-body distribution functions in condensed matter. II. Data analysis and applications, Physical Review B: Condensed Matter 52 (1995) 15135–15149, https://doi.org/10.1103/physrevb.52.15135.
[27] J. Jaumot, A. de Juan, R. Tauler, MCR-ALS GUI 2.0: new features and applications, Chemometrics and Intelligent Laboratory Systems. 140 (2015) 1–12, https://doi.org/10.1016/j.chemolab.2014.10.003.
[28] D. Fontana, L. Pietrelli, Separation of middle rare earths by solvent extraction using 2-ethylhexylphosphonic acid mono-2-ethylhexyl ester as an extractant, Journal of Rare Earths. 27 (2009) 830–833, https://doi.org/10.1016/S1002-0721(08)60344-0.
[29] S. Zamponi, M. Berrettoni, P.J. Kulesza, K. Miecznikowski, M.A. Malik, O. Makowski, R. Marassi, Influence of experimental conditions on electrochemical behavior of Prussian blue type nickel hexacyanoferrate film, Electrochimica Acta. 48 (2003) 4261–4269, https://doi.org/10.1016/j.electacta.2003.08.001.
[30] O. Makowski, J. Stroka, P.J. Kulesza, M.A. Malik, Z. Galus, Electrochemical identity of copper hexacyanoferrate in the solid-state: evidence for the presence and redox activity of both iron and copper ionic sites, Journal of Electroanalytical Chemistry. 532 (2002) 157–164, https://doi.org/10.1016/S0022-0728(02)00965-8.
[31] M. Giorgetti, L. Guadagnini, D. Tonelli, M. Minicucci, G. Aquilanti, Structural characterization of electrodeposited copper hexacyanoferrate films by using a spectroscopic multi-technique approach, Physical Chemistry Chemical Physics 14 (2012) 5527–5537, https://doi.org/10.1039/C2CP24109A.
[32] W. Li, F. Zhang, X. Xiang, X. Zhang, High-efficiency Na-storage performance of a nickel-based ferricyanide cathode in high-concentration electrolytes for aqueous sodium-ion batteries, ChemElectroChem 4 (2017) 2870–2876, https://doi.org/10.1002/celc.201700776.
[33] A.L. Lipson, S.-D. Han, S. Kim, B. Pan, N. Sa, C. Liao, T.T. Fister, A.K. Burrell, J. T. Vaughey, B.J. Ingram, Nickel hexacyanoferrate, a versatile intercalation host for

divalent ions from nonaqueous electrolytes, Journal of Power Sources. 325 (2016) 646–652, https://doi.org/10.1016/j.jpowsour.2016.06.019.
[34] Y. Avila, P. Acevedo-Peña, L. Reguera, E. Reguera, Recent progress in transition metal hexacyanometallates: from structure to properties and functionality, Coordination Chemistry Reviews. 453 (2022), 214274, https://doi.org/10.1016/j.ccr.2021.214274.
[35] A. Dostal, M. Hermes, F. Scholz, The formation of bilayered nickel-iron, cadmium-iron and cadmium—silver hexacyanoferrates by an electrochemically driven insertion—substitution mechanism, Journal of Electroanalytical Chemistry. 415 (1996) 133–141, https://doi.org/10.1016/S0022-0728(96)04709-2.
[36] M. Ciabocco, M. Berrettoni, S. Zamponi, J.A. Cox, S. Marini, Electrochemical behavior of Inhcf in alkali metal electrolytes, Journal of Solid State Electrochemistry 17 (2013) 2445–2452, https://doi.org/10.1007/s10008-013-2123-2.
[37] F. Scholz, A. Dostal, The formal potentials of solid metal hexacyanometalates, Angewandte Chemie International Edition in English. 34 (1996) 2685–2687, https://doi.org/10.1002/anie.199526851.
[38] E. Varbanova, V. Stefanova, A comparative study of inductively coupled plasma optical emission spectrometry and microwave plasma atomic emission spectrometry for the direct determination of lanthanides in water and environmental samples, Ecology & Safety. 9 (2015) 362–374.
[39] Y. Jang, C.-H. Hou, K. Kwon, J.S. Kang, E. Chung, Selective recovery of lithium and ammonium from spent lithium-ion batteries using intercalation electrodes, Chemosphere 317 (2023), 137865, https://doi.org/10.1016/j.chemosphere.2023.137865.
[40] G.A. Moldoveanu, V.G. Papangelakis, Leaching of lanthanides from various weathered elution deposited ores, Canadian Metallurgical Quarterly. 52 (2013) 257–264, https://doi.org/10.1179/1879139513Y.0000000060.
[41] W. Rudolph, G. Irmer, Hydration and ion pair formation in aqueous Lu3+-solution, Molecules 23 (2018) 3237, https://doi.org/10.3390/molecules23123237.
[42] Marcel. Maeder,, Evolving factor analysis for the resolution of overlapping chromatographic peaks, Analytical Chemistry 59 (1987) 527–530, https://doi.org/10.1021/ac00130a035.
[43] R. Tauler, Multivariate curve resolution applied to second order data, Chemometrics and Intelligent Laboratory Systems 30 (1995) 133–146, https://doi.org/10.1016/0169-7439(95)00047-X.
[44] M. Giorgetti, A. Mullaliu, P. Conti, XAFS studies on battery materials: Data analysis supported by a chemometric approach, Radiation Physics and Chemistry. 175 (2020), 108252, https://doi.org/10.1016/j.radphyschem.2019.04.002.
[45] P. D'Angelo, A. Zitolo, V. Migliorati, G. Chillemi, M. Duvail, P. Vitorge, S. Abadie, R. Spezia, Revised ionic radii of lanthanoid(III) ions in aqueous solution, Inorganic Chemistry 50 (2011) 4572–4579, https://doi.org/10.1021/ic200260r.